

Full Paper

MOCVD of KNbO_3 Ferroelectric Films and their Characterization**

By Mikhail V. Romanov,* Igor E. Korsakov, Andrey R. Kaul, Sergey Yu. Stefanovich, Ivan A. Bolshakov, and Georg Wahl

KNbO_3 in the form of films is a highly acclaimed material due to its potential application in surface acoustic wave (SAW), and nonlinear optic devices. Single-source powder flash evaporation MOCVD of epitaxial KNbO_3 films was accomplished, for the first time, with potassium *tert*-butoxide and niobium heteroligand complex, $\text{Nb}(\text{O}^i\text{Pr})_4(\text{thd})$ used as volatile metal-organic precursors. The microstructure of the films was found to be dependent on the substrate used (MgO or SrTiO_3) and deposition temperature. A new approach to reach cation stoichiometry of deposited films deficient in potassium, consisting of a post-deposition annealing with a $\text{KNbO}_3/\text{K}_3\text{NbO}_4$ powder mixture, was proposed. The device quality of the films was verified by high second harmonic generation (SHG) output. The effect of the oxygen non-stoichiometry of films on the phase transition temperature was proven.

Keywords: Isopiestic method, MOCVD, Niobium precursor, Potassium niobium oxide, Second harmonic measurements

1. Introduction

Perovskite-like pseudo-cubic oxide KNbO_3 has the same sequence of ferroelectric phase transitions (tetrahedral-orthorhombic-rhombohedral)^[1] as BaTiO_3 , but outperforms that well known ferroelectric in many technical parameters. In particular, single-crystal KNbO_3 exceeds most non-linear optical materials in the efficiency of conversion of YAG:Nd-laser radiation to its second harmonic,^[2] and also demonstrates very attractive electro-optic and electro-mechanical characteristics.^[3,4] Unfortunately, optical and acoustic applications of KNbO_3 are strongly restricted by the severe technological difficulties of single-crystal growth from flux, and subsequent conversion into single-domain state.^[4–6] However, wider application of KNbO_3 in integrated optics and SAW devices is expected if continuous KNbO_3 thin films with ferroelectric properties comparable to those of bulk material can be obtained.^[7,8]

KNbO_3 films have already been fabricated using sol-gel,^[9,10] RF sputtering,^[11,12] and pulsed laser deposition techniques.^[13,14] Although MOCVD is one of the most

technologically viable techniques, there have been only a few reports on the MOCVD of KNbO_3 films with acceptable properties, and all depositions were carried out exploiting MOCVD with the separate evaporation of individual precursors.^[15–18] An attempt to grow KNbO_3 films by single-source MOCVD was undertaken earlier,^[19] but the films were of low quality.

The major problem that makes separate evaporation necessary is the difference in melting points of commonly used precursors: potassium 2,2,6,6-tetramethylheptanedionate-3,5 ($\text{K}(\text{thd})$ $T_{\text{melt}} = 185^\circ\text{C}$) and niobium alkoxides (commonly used $\text{Nb}(\text{OEt})_5$ $T_{\text{melt}} = 6^\circ\text{C}$), as well as their tendency to cross-exchange ligands. $\text{Nb}(\text{thd})_4$, possessing a higher melting point, is also known as an alternative Nb precursor, however it is expensive and susceptible to oxidizing hydrolysis, because of the low valence state of Nb. At the same time, alkoxide heteroligand metal complexes, where one or more ligands form chelate cycles, are more stable to hydrolysis than alkoxides.^[20] Recently, there have been reports in the literature on the synthesis of such tantalum and niobium precursors for MOCVD.^[21,22]

In this study, we used niobium isopropoxide-dipivaloyl-methanate $\text{Nb}(\text{O}^i\text{Pr})_4(\text{thd})$ for KNbO_3 film deposition for the first time. Potassium *tert*-butoxide $[\text{K}(\text{O}^t\text{Bu})]_4$ and dipivaloyl-methanate $\text{K}(\text{thd})$ were used as potassium precursors, and their properties were compared.

The influence of the growth conditions on the film properties was investigated, and the ferroelectric nature of the films was confirmed by SHG measurements.

Minor variations of cation stoichiometry of the films, unavoidable in MOCVD, may strongly affect functional properties of the films, therefore a precise control of the stoichiometry of the desired phase is very important. Here, we report a method of synthesizing KNbO_3 films through a

[*] M. V. Romanov, Dr. I. E. Korsakov, Prof. A. R. Kaul, Dr. S. Yu. Stefanovich, I. A. Bolshakov
Department of Chemistry, Division of Inorganic Chemistry
Moscow State University
119899 Moscow (Russia)
E-mail: romanov@inorg.chem.msu.ru

Prof. G. Wahl
Institut fuer Oberflaechentechnik und Plasmatechnische
Werkstoffentwicklung
TU Braunschweig
Bienroder Weg 53, D-38108 Braunschweig (Germany)

[**] The authors acknowledge the kind help of Dr. A. A. Kamenev and Dr. A. A. Bosak in the TEM studies. The authors thank Dr. A. A. Molodyk and Mr. N. A. Mirin for their help in preparing the manuscript. This work was supported by VW Foundation I/77821.

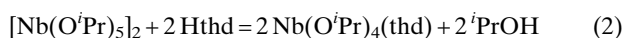
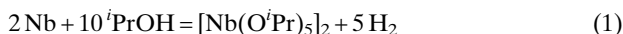
post-deposition annealing of initially potassium-deficient films in the presence of a $\text{KNbO}_3/\text{K}_3\text{NbO}_4$ mixture.

2. Results and Discussion

2.1. Precursor Synthesis and Characterization

2.1.1. Niobium Precursor

The synthetic approach adopted involved two stages, as shown in Reactions 1 and 2.



In the first stage, $[\text{Nb}(\text{O}^i\text{Pr})_5]_2$ was obtained by anodic oxidation of metallic niobium in absolute alcohol in the presence of LiCl , added to increase the electrolysis current. The product was purified by vacuum distillation. The second stage consisted of the direct reaction of alkoxide with Hthd, the product once again being purified by vacuum sublimation. All operations were carried out under dry nitrogen in closed vessels or in a glove box. The substance obtained was slightly yellowish and relatively stable to moisture, showing no signs of decomposition even after being left for several minutes in air. Its melting temperature was in the range $152\text{--}154\text{ }^\circ\text{C}$ (compared to $79\text{ }^\circ\text{C}$ for $[\text{Nb}(\text{O}^i\text{Pr})_5]_2$), permitting its use in powder flash evaporation MOCVD. In the IR spectra, the bands at $1500\text{--}1600\text{ cm}^{-1}$, corresponding to $\nu(\text{C}\cdots\text{O}$, $\text{C}\cdots\text{C})$ vibrations, clearly indicate the bidentate-chelating mode of the thd[−] ligand in the compound obtained.^[23]

2.1.2. Potassium Precursors

Kthd was prepared by neutralization in an ethanol/water solution, as per Reaction 3, and was isolated by vacuum sublimation.



IR spectroscopy indicated the formation of water adduct $\text{Kthd} \cdot x\text{H}_2\text{O}$. Our MOCVD experiments using this precursor resulted in only potassium-deficient films, even when there was a large excess of Kthd over $\text{Nb}(\text{O}^i\text{Pr})_4(\text{thd})$ (molar ratio $\text{K}/\text{Nb} = 8$) in the precursor mixture. At the same time, a fourfold excess of potassium *tert*-butoxide was enough to obtain the proper K/Nb ratio in the films. It is to be noted that some residue always remains after the evaporation of Kthd as well as $[\text{K}(\text{O}^i\text{Bu})_4]$.

With volatile alkaline metal compounds, we encountered the same problem that is well-known for volatile complexes of alkaline earth metals; the volatile properties of compounds with the generic formula $\text{M}(\beta\text{-diketonate})$ (where

M = alkaline metal) are discussed in detail elsewhere.^[24] A coordination sphere of potassium in Kthd is highly unsaturated, so the complex tends to saturate it with miscellaneous molecules which are often solvent molecules, e.g., water. Also, these unoccupied sites facilitate intermolecular bonding leading to poor volatility. These factors significantly decrease the volatility of Kthd, making it unsuitable as a precursor in terms of vapor pressure value and stability.

On the other hand, $[\text{K}(\text{O}^i\text{Bu})_4]$ has a more stable, cubane-like tetrameric structure (Fig. 1), thanks to which this compound is more stable in storage and is less susceptible to degradation during sublimation. Its high melting point of $256\text{ }^\circ\text{C}$ allows it to sublime without melting. That is an advantage since, in melt, all degradation processes are accelerated.

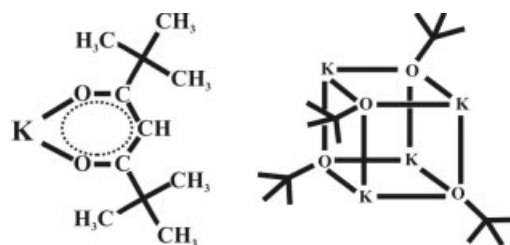


Fig. 1. Molecular structure diagrams of Kthd and $[\text{K}(\text{O}^i\text{Bu})_4]$ [25].

2.2. MOCVD of KNbO_3 Films

KNbO_3 films were deposited using either the powder flash evaporation technique,^[26] or aerosol-source MOCVD in the system schematically shown in Figure 2. During aerosol-source MOCVD experiments, we observed that the solution containing $\text{Nb}(\text{O}^i\text{Pr})_4(\text{thd})$ and $[\text{K}(\text{O}^i\text{Bu})_4]$,

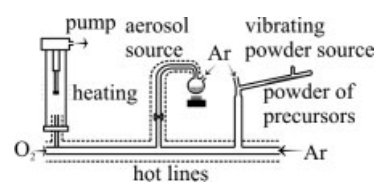


Fig. 2. Scheme of an MOCVD system.

initially transparent and colorless, turned white after a short time and the precursors began to precipitate out. This may have happened as a result of a ligand exchange reaction in the solution. Deposition using that solution resulted in potassium-deficient films.

During powder flash evaporation MOCVD experiments, the reactor was heated with an RF-inductor (cold-wall reactor) or, in the other experiments, with a resistive furnace (hot-wall reactor). In the case of the hot-wall reactor, we found it difficult to avoid the formation of gas-phase nucleated particles. At a thickness of about $1\text{ }\mu\text{m}$ and higher, the films became opaque because of incorporated particles. We believe these particles appear due to homogeneous nucleation arising from the thermal instability of the precur-

sors' vapor during the increased residence time in the heated zone of the hot-wall reactor. Finally optimum conditions for obtaining KNbO_3 films were found to be in the cold-wall reactor using powder flash evaporation MOCVD and $\text{K}(\text{O}^i\text{Bu})$ and $\text{Nb}(\text{O}^i\text{Pr})_4(\text{thd})$ as precursors. Deposition conditions are summarized in Table 1.

Table 1. MOCVD growth conditions of KNbO_3 films.

Deposition temperature [$^{\circ}\text{C}$]	700–800
Heated lines temperature [$^{\circ}\text{C}$]	180–200
Total pressure ($\text{Ar}+\text{O}_2$) [mbar]	10–13
O_2 pressure [mbar]	5.0–6.5
Growth rate [nm min^{-1}]	30–60

2.2.1. Film Composition

The correct composition of precursor mixture is necessary for the deposition of stoichiometric films. Figure 3 shows the correspondence of the cation ratios in the precursor mixtures to those in the films grown under the same

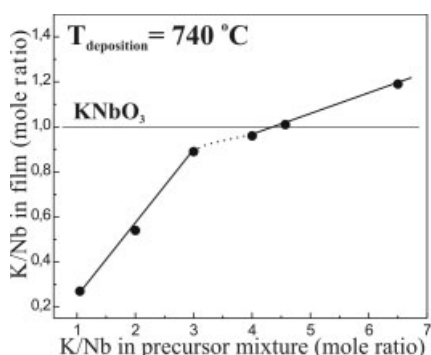


Fig. 3. The relationship between K/Nb molar ratio in the film and the precursor mixture.

conditions. K:Nb ratio in the precursors was set by precise weighing of the precursor powders, while the cation ratio of the films was determined using energy dispersive X-ray (EDX) analysis.

The sublimation of potassium *tert*-butoxide always leaves a residue, apparently due to slow degradation processes that lead to the formation of nonvolatile compounds. K_2O is known to be volatile at high temperatures, so to obtain stoichiometric films, it is necessary to use an excess of potassium precursor in the source mixture. Stoichiometric KNbO_3 films were obtained in-situ, only when the composition $[\text{K}(\text{O}^i\text{Bu})]_4/\text{Nb}(\text{O}^i\text{Pr})_4(\text{thd}) = 4$ was used. The slope of the graph in Figure 3 alters when K:Nb in the film approaches unity, evidence of a change in the sorption-desorption kinetic of K_2O . Similar, but more pronounced, behavior was noticed earlier for the deposition of Pb-containing materials where a slight excess of lead oxide could readily vaporize from the growing film but could not be incorporated into the film.^[27]

2.2.2. A Method of Reaching the Proper K:Nb Ratio in the Film

To reach the proper K:Nb ratio in potassium-deficient films, we proposed to use a post-deposition annealing of the films in a covered crucible where potassium oxide vapor pressure is set by coexisting $\text{K}_3\text{NbO}_4/\text{KNbO}_3$ phases. This approach is known as the isopiestic method. The equilibrium mixture of $\text{K}_3\text{NbO}_4/\text{KNbO}_3$ was obtained by conventional ceramic synthesis. On the basis of the phase diagram of the quasibinary system $\text{K}_2\text{O}/\text{Nb}_2\text{O}_5$ (Fig. 4) and Gibb's phase rule, it can be stated that, in the equilibrium gas phase, this mixture sets up the chemical potential of K_2O , which is sufficient for the formation of a KNbO_3 phase containing the maximum activity of K_2O . At high

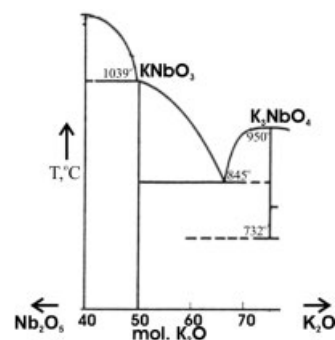


Fig. 4. Part of the $\text{K}_2\text{O}/\text{Nb}_2\text{O}_5$ phase diagram [28].

temperatures, K_2O readily transports through the gas phase from a powder mixture of $\text{K}_3\text{NbO}_4/\text{KNbO}_3$ and saturates the film until the proper stoichiometry is reached. Thus, the films with an initial ratio $\text{K}/\text{Nb} < 1$, after attaining equilibrium with this mixture, should form KNbO_3 . This was proven with the results of quantitative EDX analysis, i.e., EDX analysis of an initially potassium-deficient film gave the K/Nb ratio 0.27. After one hour annealing at 750°C with $\text{K}_3\text{NbO}_4 + \text{KNbO}_3$, the value of this ratio became 1.06, which is very close to that (1.05) for the standard bulk crystal of KNbO_3 . Consequently, a stoichiometric KNbO_3 film was formed.

2.3. X-ray Diffraction (XRD)

The phase compositions of the as-deposited films and those annealed with $\text{K}_3\text{NbO}_4 + \text{KNbO}_3$ powder were investigated using XRD. The θ - 2θ scan of an as-grown potassium-deficient film in Figure 5a reveals the peaks of KNbO_3 (110) and (220), together with some reflections of a secondary phase, $\text{K}_x\text{Nb}_y\text{O}_z$ (where $x/y < 1$). The latter is difficult to assign unambiguously to a given phase, but after the annealing, the reflections of the secondary phase disappeared, and only KNbO_3 reflections were present (Fig. 5b). Thus, a single-phase oriented film of KNbO_3 was obtained.

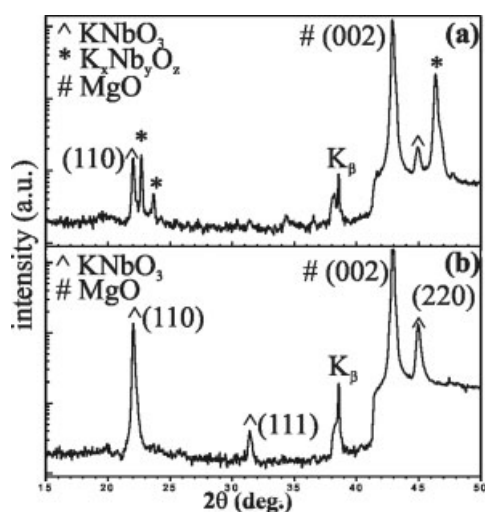


Fig. 5. θ - 2θ XRD scans. a) As-grown film deficient in potassium. b) The same film annealed with a powder mixture of K_3NbO_4 and KNbO_3 .

Using the growth conditions reported in Table 1, stoichiometric single-phase KNbO_3 films were deposited by MOCVD on $\text{MgO}(100)$, $\text{SrTiO}_3(100)$, and $\text{SrTiO}_3(110)$ substrates after the trial precursor ratio optimization. On (001) oriented substrates, (110) oriented films grew, that is equivalent to $(001)_p$ orientation in pseudocubic notation (Fig. 6), and $(110)_p$ oriented films grew on $\text{SrTiO}_3(110)$. At room temperature, bulk KNbO_3 has orthorhombic unit cell

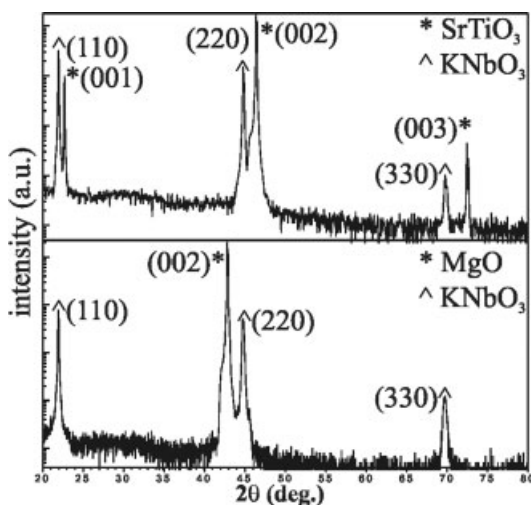


Fig. 6. θ - 2θ XRD scans for an epitaxial (110) MOCVD-derived KNbO_3 films on $\text{SrTiO}_3(001)$, $\text{MgO}(001)$.

with the following parameters: $a = 5.695 \text{ \AA}$, $b = 5.721 \text{ \AA}$, $c = 3.973 \text{ \AA}$,^[29] (the polarization vector \mathbf{P}_s is parallel to the b axis). Within the accuracy of the measurement, we did not observe any difference between the lattice spacing of the KNbO_3 films and the bulk values. It is noted that the shortest axis (the c axis) lies in the plane of the substrate. This agrees well with the results obtained by other authors, and was ascribed earlier to the fact that it is energetically

favorable for this axis to remain in the plane of the substrate because its length stays constant during phase transitions.^[30]

X-ray ϕ scans were examined in order to determine in-plane alignment of the samples. They proved the cube-on-cube epitaxy of the films on (001)-oriented MgO and SrTiO_3 substrates, illustrated in Figure 7 with ϕ scans of $\text{KNbO}_3\{220\}_p$ and $\text{SrTiO}_3\{220\}$ reflections. Figure 8 shows that the full width at half maximum (FWHM) value of the rocking curve of the film on MgO is significantly larger than that for the film on the SrTiO_3 substrate, due to the larger mismatch in the case of MgO . The mismatch for $\text{KNbO}_3[110] \parallel \text{substrate}[001]$ is 6.0 % and 3.3 % for MgO and SrTiO_3 , respectively.

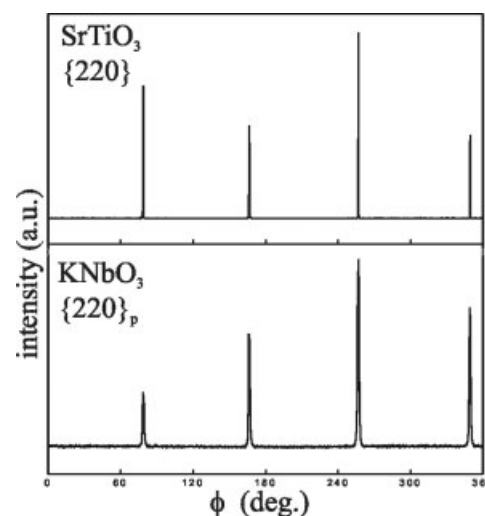


Fig. 7. X-ray ϕ scan for an epitaxial (110) KNbO_3 film deposited on $\text{SrTiO}_3(001)$.

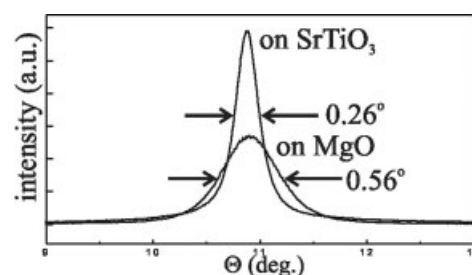


Fig. 8. Rocking curves ($\text{KNbO}_3(110)$ reflection) of KNbO_3 films on $\text{MgO}(001)$ and $\text{SrTiO}_3(001)$ substrates.

2.4. Scanning Electron Microscopy (SEM) and Transmission Electron Microscopy (TEM)

An SEM study was performed for the films grown on various substrates under varying conditions. Figure 9 depicts the morphologies of films deposited on MgO substrates at varying temperatures. That recrystallization is enhanced by increasing deposition temperature is indicated by the film crystallites becoming larger, and the pores coalescing. It is

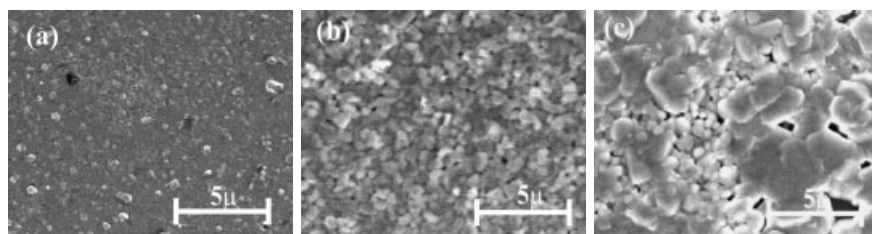


Fig. 9. SEM images of KNbO₃ films on MgO. a) $T_{\text{dep}} = 700^\circ\text{C}$. b) $T_{\text{dep}} = 740^\circ\text{C}$. c) $T_{\text{dep}} = 800^\circ\text{C}$.

probable that the pores form due to K₂O evaporation during film growth. However, although they are also porous, the films on SrTiO₃ substrates, even those deposited at $T_{\text{dep}} = 740^\circ\text{C}$, do not contain crystallites (Fig. 10), evidently due to better coherence at the film/substrate interface.

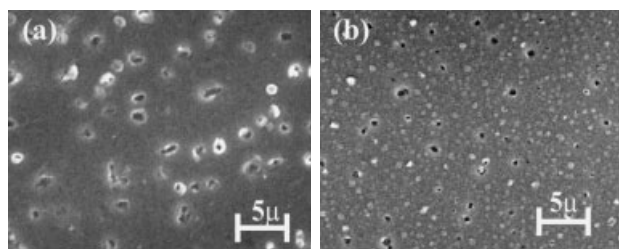


Fig. 10. SEM images of KNbO₃ films on SrTiO₃. a) $T_{\text{dep}} = 700^\circ\text{C}$. b) $T_{\text{dep}} = 740^\circ\text{C}$.

Cross-section studies of KNbO₃ films on SrTiO₃(110) were performed using TEM, and the representative results for one of these studies are shown in Figure 11a–c. According to θ – 2θ X-ray data, this film showed a (011)_p orientation. The film had a columnar structure, and was dense up to a thickness of $\sim 0.4\ \mu\text{m}$. In the upper portion of the film (at $0.4\ \mu\text{m}$ thickness and above), there are columns separated by voids. A high-resolution (HR) TEM image of a boundary between the columns in the dense part of the film is shown in Figure 11b. This boundary does not change the orientation of neighboring film blocs (thus, this is not a low angle boundary). However there is a shift of atomic planes along the [011]_p-axis that is clearly shown in the Fourier transform image in Figure 11c. This extended defect can be classified as an antiphase boundary, or crystallographic shear plane. In the latter case, the occurrence of this defect

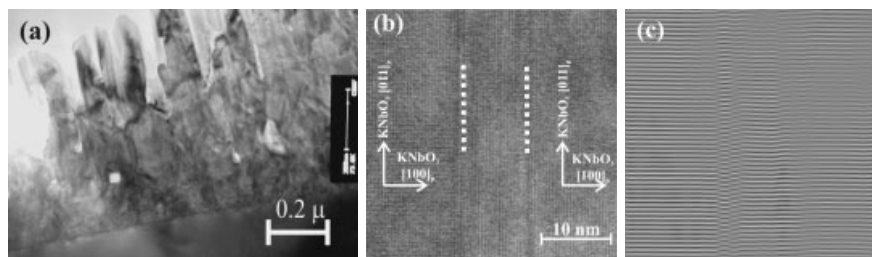


Fig. 11. TEM images of KNbO₃/SrTiO₃(011). a) Low magnification image. b) Image of extended defect. c) Fourier-transform image of the defect shown in (b).

should be associated with oxygen non-stoichiometry. Crystallographic shear planes are common defects in niobium oxide,^[31] but the presence of shear plane-type defects in a complex niobium oxide with perovskite structure has, to our knowledge, never been reported. The nature of these extended defects in KNbO₃ films needs further investigation.

2.5. Second Harmonic Measurements

Our investigation of second harmonic generation (SHG) in KNbO₃ films was done without any poling, so the samples under study had their original microdomain structure. Taking into account that the film thickness is smaller than coherency length in KNbO₃ (we can disregard the effects of phase synchronism), and that there can be several ferroelectric domains across the film thickness (we assume that in each domain the second harmonic is generated independently), the SHG intensity can be approximated by Equation 4.

$$I_{2\omega} \sim I_{\omega}^2 d_{\text{av}}^2 I_{\text{d}}^2 N \quad (4)$$

d_{av} and I_{d} denote the average nonlinear coefficient and domain size, respectively, and N is the number of domains along the pathway of the laser beam through the film. Because N is simply related to the film thickness H , as $N = H/I_{\text{d}}$ the expression above can be written as Equation 5.

$$I_{2\omega} \sim I_{\omega}^2 d_{\text{av}}^2 I_{\text{d}} H \quad (5)$$

Thus, the magnitude of SHG gives information about the existence of independent ferroelectric domains in the films. Changes in spontaneous polarization that happen at phase transitions can be followed using a temperature dependence of SHG through the relation $d_{\text{av}} \sim P_{\text{s}}$.^[32]

The temperature dependence of SHG intensity for an as-grown epitaxial KNbO₃ film on SrTiO₃(001) is shown in Figure 12a. The sequence of transitions between cubic, tetragonal, and orthorhombic phases is clearly seen in this graph. The step-like drops at 163 – 184°C and 389°C in

Figure 12a correspond to phase transitions from orthorhombic to tetragonal, and from tetragonal to cubic phase, respectively. The temperatures of phase transitions were determined at the middle of steep drops of $I_{2\omega}(T)$ curves. The transition temperatures we observed were remarkably low compared to the values for KNbO₃ bulk crystals (435°C and 225°C for $m3m \rightarrow mm4 \rightarrow mm2$ transitions, respectively). We attribute this discrep-

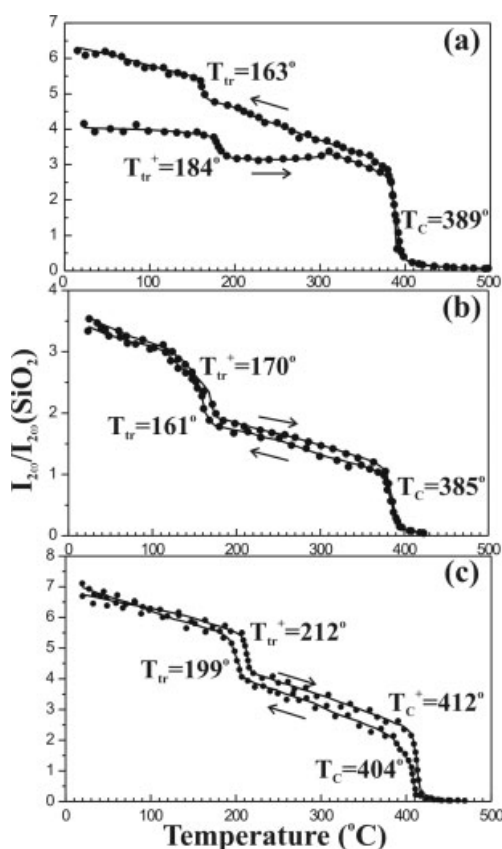


Fig. 12. Temperature dependence of SHG signal in KNbO₃ films; a) as-grown, b) annealed in Ar, c) annealed in O₂.

ancy to the oxygen or cation non-stoichiometry in as-grown films, which is undetectable in lattice spacing shift by XRD analysis. Heating and cooling curves in Figure 12a have different slopes, and in the heating-cooling cycle the SHG intensity increased by a factor of 1.5. Because of the non-linear optical coefficient decreasing with temperature in KNbO₃, heating should be associated with the suppression of $I_{2\omega}$.^[33] However, we did not observe such an effect, probably because of changes in domain microstructure during the heating process. According Equation 4, the enlarging of the ferroelectric domains should result in an increase in SHG intensity.

To verify the effect of oxygen non-stoichiometry of the film on phase transition temperatures, we performed $I_{2\omega}(T)$ measurements after the sequential annealing of this sample in reducing (Ar) and oxidizing (O₂) atmospheres.

The one hour treatment in argon at 500 °C did not change the temperatures of phase transitions significantly (Fig. 12b). In contrast, after the treatment in oxygen (1 h, 500 °C) the phase transition temperatures increased by about 25 °C (Fig. 12c). We believe that partial compensation of the oxygen non-stoichiometry was achieved during the oxidation. However, the difference in the phase transition temperatures between the film and the bulk material

was present, apparently due to residual oxygen non-stoichiometry. If the defects observed in the films by TEM (Fig. 11) are crystallographic shear planes, then their presence is further evidence of non-stoichiometry. Obviously, these defects cannot be completely remedied by the oxidizing annealing under the rather soft conditions that we used. It should be noted that all $I_{2\omega}$ vs. T graphs displayed temperature hysteresis of the phase transitions. This behavior is typical for the first order phase transitions in KNbO₃.^[5] The intensity of SH signal from a 2 μm thick film was of the order of 1 % of the intensity from a single grain-thick powder sample of KNbO₃ consisting of single-domain grains with the dimensions ~3 μm. Hence, Equation 5 allows the average domain size estimation in KNbO₃ films $l_d \approx 0.05$ μm, which is in good agreement with the size of the domains observed earlier in plane view TEM images of KNbO₃ films.^[34]

3. Conclusions

Epitaxial KNbO₃ films were obtained for the first time by single, solid-source MOCVD. A method of post-deposition annealing of potassium-deficient films, in order to obtain films with proper cation stoichiometry, was proposed. The surface morphology of the films grown on various substrates was investigated. Columnar microstructure and extended defects were observed by HRTEM in the films on SrTiO₃.

SHG experiments confirmed that ferroelectric properties of the films were very similar to those in bulk KNbO₃, although oxygen non-stoichiometry strongly influenced the temperature of phase transitions in KNbO₃ films. Oxygen stoichiometry can be partially restored by annealing the samples in soft oxidizing conditions.

Further work on this system is in progress. In the future, we will attempt to test such films in prototype opto-electronic and acousto-electronic devices.

4. Experimental

Synthesized Nb(O'Pr)₄(thd) was characterized by gravimetry, elemental analysis, and IR spectroscopy. Anal. Calcd. for C₂₃H₄₇O₆Nb: C 53.9, H 9.2, Nb₂O₅ 25.98. Found: C 54.3, H 10.0, Nb₂O₅ 25.81. IR [cm⁻¹]: 3200–3550 w br, 2969 m, 2929 m, 2875 m, 1592 s, 1574 s, 1554 s, 1534 s, 1504 s, 1464 vs m, 1386 vs m, 1374 w, 1358 s br, 1328 s, 1294 w, 1248 m, 1227 m, 1179 w, 1162 s, 1127 s br, 998 s br, 938 m, 874 m, 850 s, 794 m, 766 w, 739 w, 722 w, 595 s br, 498 w, 481 w, 420–474 w. The presence of OH⁻ valency vibrations in 3200–3600 cm⁻¹ is probably due to the partial hydrolysis during the probe preparation for the spectroscopy. $T_{\text{melt}} = 152\text{--}154$ °C.

Deposited films were characterized by means of XRD, SEM, EDX, and SHG output. θ – 2θ , φ scans, and rocking curves were measured using a Siemens D5000 four-circle diffractometer. SEM and EDX analyses were performed using a Jeol 840A and Camscan-4m electron microscopes; a crystal of potassium niobium oxide was used as a standard for quantitative analysis. Carbon was deposited on the samples before EDX analysis was carried out. SHG film examination was carried out using a YAG:Nd laser according to

the reflection scheme. Both the directions of laser beam and second harmonic registration were at 90° to the sample surface. A powder sample of crushed α -quartz was used as a reference. To study phase transitions, SHG experiments were performed during heating and cooling of the samples at the rate of about 5 °C min⁻¹.

Received: October 21, 2003
Final version: February 20, 2004

- [1] G. Shirane, H. Danner, A. Pavlovic, R. Pepinsky, *Phys. Rev.* **1954**, 96, 672.
- [2] D. Fluck, J. Moll, P. Günter, M. Fleuster, C. Buchal, *Electron. Lett.* **1992**, 28, 1092.
- [3] M. Zgonik, R. Schlessler, I. Biaggio E. Voit, J. Tscherry, P. Gunter, *J. Appl. Phys.* **1993**, 74, 1287.
- [4] K. Yamanouchi, Y. Wagatsuma, H. Odagawa, Y. Cho, *J. Eur. Ceram. Soc.* **2001**, 21, 2791.
- [5] S. Wada, A. Seike, T. Tsurumi, *Jpn. J. Appl. Phys. Part 1* **2001**, 40, 5690.
- [6] U. Flückiger, H. Arend, *J. Cryst. Growth* **1978**, 43, 406.
- [7] M. H. Francombe, in *Physics of Thin Films* (Eds. M. H. Francombe, J. L. Vossenc), Academic Press, San Diego, CA **1993**, p. 225.
- [8] B. W. Wessels, *J. Cryst. Growth* **1998**, 195, 706.
- [9] H. Endo, M. J. Cima, *Mater. Res. Soc. Symp. Proc.* **1993**, 310, 325.
- [10] S. L. Swartz, P. J. Melling, C. S. Grant, *Mater. Res. Soc. Symp. Proc.* **1989**, 152, 227.
- [11] S. Schwyn Thony, H. W. Lehmann, *Appl. Phys. Lett.* **1992**, 61, 373.
- [12] S. R. Sashital, S. Krishnakamur, S. Esener, *Appl. Phys. Lett.* **1993**, 62, 2917.
- [13] L. S. Hung, L. A. Bosworth, *Appl. Phys. Lett.* **1993**, 62, 2625.
- [14] C. Zaldo, D. S. Gill, R. W. Eason, J. Mendiola, P. J. Chandler, *Appl. Phys. Lett.* **1994**, 65, 502.
- [15] M. J. Nystrom, B. W. Wessels, D. B. Studebaker, T. J. Marks, W. P. Lin, G. K. Wong, *Appl. Phys. Lett.* **1995**, 67, 365.
- [16] M. J. Nystrom, B. W. Wessels, J. Chen, T. J. Marks, *Appl. Phys. Lett.* **1996**, 68, 761.
- [17] A. Onoe, A. Yoshida, K. Yoshida, *Appl. Phys. Lett.* **1996**, 69, 167.
- [18] A. Onoe, A. Yoshida, K. Chikuma, *Appl. Phys. Lett.* **2001**, 78, 49.
- [19] R. Hiskes, S. A. Dicarolis, J. Fouquet, R. K. Route, R. S. Feigelson, F. Leplingard, *Mater. Res. Symp. Proc.* **1994**, 335, 299.
- [20] N. Y. Turova, E. P. Turevskaya, V. G. Kessler, M. I. Yanovskaya, *The Chemistry of Metal Alkoxides*, Kluwer Ac., Dordrecht, The Netherlands **2001**, p. 403.
- [21] H. W. Davies, T. J. Leedham, A. C. Jones, P. O'Brien, A. J. P. White, D. J. Williams, *Polyhedron* **1999**, 18, 3165.
- [22] P. W. Williams, A. C. Jones, P. J. Wright, M. J. Crosbie, J. F. Bickley, A. Steiner, H. O. Davies, T. J. Leedham, *Chem. Vap. Deposition* **2002**, 8, 110.
- [23] K. Nakamoto, *Infrared and Raman Spectra of Inorganic and Coordination Compounds*, 4th ed., John Wiley & Sons, Chichester, UK **1986**.
- [24] R. Belcher, A. W. L. Dudeney, W. I. Stephen, *J. Inorg. Nucl. Chem.* **1969**, 31, 625.
- [25] M. H. Chisholm, S. R. Drake, A. A. Naiini, W. E. Streib, *Polyhedron* **1991**, 10, 337.
- [26] A. A. Molodyk, I. E. Korsakov, M. A. Novojilov, I. E. Graboy, A. R. Kaul, G. Wahl, *Chem. Vap. Deposition* **2000**, 6, 133.
- [27] A. A. Bosak, A. N. Botev, O. Y. Gorbenco I. E. Graboy, S. V. Samoilenkov, A. R. Kaul, C. Dubourdiou, J. P. Senateur, *J. Phys. IV* **2001**, 11, Pr 3-93.
- [28] A. Reismann, F. Holtzberg, *J. Am. Chem. Soc.* **1955**, 77, 2117.
- [29] Joint Committee for Powder Diffraction Standards (JCPDS), File No. 32-0822, International Center for Diffraction Data, Newtown Square, PA **1980**.
- [30] A. F. Chow, D. J. Lichtenwalner, R. R. Woolcott, T. M. Graettinger, O. Auciello, A. I. Kington, L. A. Boatner, N. R. Parikh, *Appl. Phys. Lett.* **1994**, 65, 1073.
- [31] B. M. Gatehouse, A. D. Wadsley, *Acta Crystallogr.* **1964**, 17, 1545.
- [32] S. K. Kurtz, T. T. Perry, *J. Appl. Phys.* **1968**, 39, 3798.
- [33] V. Gopalan, R. Raj, *Appl. Phys. Lett.* **1996**, 68, 1323.
- [34] V. Gopalan, R. Raj, *J. Appl. Phys.* **1997**, 81, 865.